

2008

## Enzymatic Processing of Amelogenin during Continuous Crystallization of Apatite

Vuk Uskoković

*Chapman University, uskokovi@chapman.edu*

M.-K. Kim

*University of California - San Francisco*


W. Li

*University of California - San Francisco*

S. Habelitz

*University of California - San Francisco*

Follow this and additional works at: [https://digitalcommons.chapman.edu/pharmacy\\_articles](https://digitalcommons.chapman.edu/pharmacy_articles)

 Part of the [Biochemistry Commons](#), [Endodontics and Endodontology Commons](#), [Enzymes and Coenzymes Commons](#), [Genetic Phenomena Commons](#), [Genetic Processes Commons](#), and the [Medical Biochemistry Commons](#)

### Recommended Citation

Uskoković V, Kim M-K, Li W, Habelitz S. Enzymatic processing of amelogenin during continuous crystallization of apatite. *J Mater Res.* 2008;23(12):3184-3195. doi:10.1557/JMR.2008.0387.

This Article is brought to you for free and open access by the School of Pharmacy at Chapman University Digital Commons. It has been accepted for inclusion in Pharmacy Faculty Articles and Research by an authorized administrator of Chapman University Digital Commons. For more information, please contact [laughtin@chapman.edu](mailto:laughtin@chapman.edu).

---

# Enzymatic Processing of Amelogenin during Continuous Crystallization of Apatite

## Comments

This is a pre-copy-editing, author-produced PDF of an article accepted for publication in *Journal of Materials Research*, volume 23, issue 12, in 2008 following peer review. The definitive publisher-authenticated version is available online at DOI: [10.1557/JMR.2008.0387](https://doi.org/10.1557/JMR.2008.0387).

## Copyright

Cambridge University Press

Published in final edited form as:

*J Mater Res.* 2008 December ; 23(12): 3184–3195. doi:10.1557/JMR.2008.0387.

## Enzymatic Processing of Amelogenin during Continuous Crystallization of Apatite

V. Uskoković<sup>1</sup>, M.-K. Kim<sup>1,2</sup>, W. Li<sup>3</sup>, and S. Habelitz<sup>1</sup>

<sup>1</sup> *Division of Biomaterials and Bioengineering, Department of Preventive and Restorative Dental Sciences, University of California, San Francisco*

<sup>2</sup> *Department of Molecular and Cell Biology, University of California, Berkeley*

<sup>3</sup> *Department of Oral and Craniofacial Sciences, University of California, San Francisco*

### Abstract

Dental enamel forms through a protein-controlled mineralization and enzymatic degradation with a nanoscale precision that new engineering technologies may be able to mimic. Recombinant full-length human amelogenin (rH174) and a matrix-metalloprotease (MMP-20) were employed in a pH-stat titration system that enabled a continuous supply of calcium and phosphate ions over several days, mimicking the initial stages of matrix processing and crystallization in enamel in-vitro. Effects on the self-assembly and crystal growth from a saturated aqueous solution containing 0.4 mg/ml rH174 and MMP-20 with the weight ratio of 1:1000 with respect to rH174 were investigated. A transition from nanospheres to fibrous amelogenin assemblies was facilitated under conditions that involved an interaction between rH174 and the proteolytic cleavage products. Despite continuous titration, the levels of calcium exhibited a consistent trend of decreasing, thereby indicating its possible role in the protein self-assembly. This study suggests that mimicking enamel formation in-vitro requires the synergy between the aspects of matrix self-assembly, proteolysis and crystallization.

### Introduction

Amelogenesis is one of the most fascinating mineralization processes in the biological realm. Not only does it produce the hardest tissue among vertebrates, but it is also a process in which the extracellular matrix disintegrates in parallel with giving rise to a 96 – 98 wt% mineralized tissue with an extraordinary superstructural organization. Mature enamel is composed of 40 – 60 nm wide and up to several hundred microns long hydroxyapatite (HAP) fibers packed in a parallel fashion within rod-shaped structures of 4 – 6  $\mu\text{m}$  width<sup>1</sup> (Fig.1). Having length-to-width aspect ratios of up to 10,000, HAP crystals in enamel are 1000 times longer than the ones found in bone.

Another impressive feature of amelogenesis is that it presents a form of extracellular mineralization. Ameloblast cells secrete the majority of the ingredients of this matrix, but the nucleation, crystal growth and the subsequent locking in space of fibrous HAP crystals is implicitly assumed to be primarily under control of the self-assembling polypeptide gel. It is exactly this minimal involvement of the cell that opens the door for biomimicry studies that exclude the presence of relevant cell and tissue cultures.

Ninety weight percent of the peptide component of the enamel matrix are composed of amelogenin (Amg) proteins, while the rest mostly belongs to ameloblastin, enamelin and proteolytic enzymes. We have limited our studies to the use of only two out of a multitude of peptide species existing at one time or another during the up to four years long period of the

formation of the tooth crown and of the activity of its parenting matrix. These are a recombinant full-length human Amg (rH174) and matrix metalloprotease-20 (MMP-20), also known as enamelysin. The former comprises 90 % of all the amelogenins in the enamel matrix, and the latter is regarded as the major protease involved in the hydrolysis of Amg. MMP-20 is known to selectively cleave the full-length protein at seven sites along its sequence, but the purpose of this selective hydrolysis is still unclear. The second major enzyme, enamel matrix serine protease-1 (EMSP1), also known as kallikrein-4, increases in concentration towards the end of enamel maturation and is assumed to have the role of fully digesting Amg (as evidenced by its aggressive and less selective cleavage). On the other hand, MMP-20 is present in the enamel matrix from the earliest stages of enamel formation<sup>2</sup>, which implies that its role in the process must be more than mere digestion and promotion of the free space for the mineral expansion. In fact, the initially secreted nascent proteins are present in the enamel matrix in transient forms, and are relatively quickly processed to generate a wide spectrum of smaller peptides. It is the aim of our study to explore the role that this enzymatic reaction plays in the context of the enamel matrix maturation and the buildup of the actual crystal structure.

It has previously been evidenced that Amg forms nanospheres in aqueous solutions. Although such morphologies could be explained by the mainly hydrophobic nature of the constitutive amino acids, it is still not confirmed that these morphologies of Amg are the ones that play the role in directing the growth and spatial arrangement of HAP crystals in the developing enamel matrix. Nonetheless, as of today, the general explanation of Amg-guided crystal growth of fibrous HAP crystals in the enamel refers to a selective attachment of hydrophobic Amg nanospheres onto (hk0) planes of the growing crystals, fostering thereby their growth along [001] axis. However, fibrous assemblies of Amg, evidenced on a few previous occasions<sup>3,4,5</sup>, suggest that a mutual elongation of the inorganic and organic phases may be essential for the whole process. Therefore, a particular emphasis in our study has been placed on determining the conditions that may trigger the formation of fibrous morphologies of the protein assemblies.

As suggested by others, the cleavage products of the enzymatic reaction involving MMP-20 and the nascent Amg may play a role in facilitating the proper self-assembly of the developing enamel matrix<sup>6</sup>. This viewpoint is supported by many medical studies which showed that mutations not only on the amelogenin gene, but on the one that codes for MMP-20 cause *amelogenesis imperfecta*, i.e., a pathological state typified by the formation of abnormal and significantly weakened enamel<sup>7,8</sup>. The major hypothesis deduced from the essential role proposed for MMP-20 in regulating the mechanism of enamel formation consequently refers to a synergy between the three aspects of the process - protein self-assembly, proteolytic action and crystallization – as responsible for the proper growth of enamel at the micro scale (Fig.2). Studies of these separate aspects are thus required as much as studies of their acting in unison for a proper understanding of the mechanism of concern. The aim of this work is to provide results that would support the meaningfulness of pursuing such an integrative study.

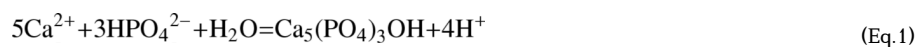
## Experimental

The recombinant rH174, rH163 and rH-MMP-20 were obtained through their expression in BL21DE3 plysS *Escherichia Coli* using a procedure described previously<sup>9</sup>. The experiments in static conditions involved rH174 dispersions in water (0.1 – 0.4 mg/ml), mixtures of rH174 and rH163 (0.1 mg/ml), or mixtures of rH174 (0.4 mg/ml) and MMP-20 (1:1000 weight ratio respective to rH174) at different pHs and in the presence of: 150 mM KCl to maintain the physiological background ionic strength; 0.02 % of NaN<sub>3</sub> as the antimicrobial agent; and 20 mM Bis-Tris/HCl or Tris/HCl as the buffer at pHs between 5 and 6.5 and 7 to 8.5, respectively. The samples were incubated at the physiological temperature, and after different aging times deposited on glass substrates, incubated in a wet cell, washed, dried with canned air and analyzed.

The experiments in the dynamic, titration mode involved the use of the so-called “constant solution composition” titration. The method was developed by Nancollas *et al* earlier<sup>10</sup>. The major difference of our titration setting from this classical one is a considerably larger amount of the peptides employed and correspondingly smaller reaction volumes (2 – 6 ml). In addition, the method was not applied in a CO<sub>2</sub>- and carbonate-free environment. As a result, selective binding and complexation of ions by the peptide species and the precipitation of a carbonated apatite imply a difficult control over the ionic concentrations. The classical constant solution composition method was designed to determine the thermodynamic data of nucleation and crystallization of various mineral systems, and thus required a perfect steadiness of the ionic conditions. In contrast, the pH-controlled titration process applied herein does not aim to keep the ionic concentrations constant over the entire reaction time, but is designed to continuously supply the solution with calcium, phosphate and hydroxyl ions in association with a pH decrease registered at a glass electrode. While continuously supplying the solution with the precipitating ions, the goal of this approach is to maintain the degree of saturation of the solution in the metastable range with regards to HAP, and thus allow the crystal growth to occur continuously but at the same time preventing a spontaneous precipitation. Accordingly, the approach presented here is termed “continuous crystallization” approach, contrasting a static approach with a continuous depletion in mineralizing ions until the equilibrium saturation is obtained and crystal growth halted.

Previous studies have shown that the degrees of saturation (DS) of 12.5 and above lead to an unselective nucleation of the apatite phase outside of the range of the provided apatite surface as part of the substrate<sup>11</sup>. The DS was calculated as equal to  $pK_{sp} - pIP$ , with  $pK_{sp}$  as the negative logarithm of the solubility activity product of stoichiometric HAP ( $pK_{sp} = 58.6$ )<sup>12</sup> and  $pIP$  as the negative logarithm of the ionic activity product. Software developed by M. J. Larsen<sup>13</sup> has been applied for calculating the ionic activity products under the conditions used in our experiments. Precipitation of the stoichiometric HAP releases 4 protons per formula unit (Eq. 1), but this drop in pH is prevented by the titration of the basic precursor solutions, triggered whenever the pH falls below the limits of the control point (set to pH 7.400). A feedback-based control is thus established between the precipitation and the titration. The basic setting of the titration system is shown in Fig.3. The concentrations of the titrant solutions were calculated using ionpair and complex formation constants, mass balance and electroneutrality expressions derived by Nancollas *et al*<sup>14</sup>. An effective titrant concentration of  $C_{eff} = 1.0$  mM was chosen with one titrant solution comprising 8.2 mM CaCl<sub>2</sub> and 284 mM KCl and the second one consisting of 5 mM KH<sub>2</sub>PO<sub>4</sub> and 7 mM KOH. The reaction vessel solution initially comprised 0.4 mg/ml rH174, 0.04 µg/ml MMP-20, 150 mM KCl, 0.02 % NaN<sub>3</sub>, 1.6 mM CaCl<sub>2</sub> and 1.0 mM KH<sub>2</sub>PO<sub>4</sub>. MMP-20 was the last component introduced to the system, thereby marking the beginning of the reaction time. The DS was calculated as equal to 10.9 with respect to pure HAP, but the presence of carbonates in the system implies the likelihood of the formation of carbonated hydroxyapatite. The pH-stat titration was performed using a Titrino 751 GDP device connected to a Dosimat 755 (*Brinkmann-Metrohm*) with 1 ml burettes. Micro-glass electrodes from *Metrohm* were used for monitoring the pH.

The experiments were carried out throughout 7-day periods of time. Three experimental runs for each test group were performed, which included: a) without rH174; b) with 0.4 mg/ml rH174; and c) with 0.4 mg/ml rH174 and MMP-20 (1000:1 weight ratio respective to rH174). Polished and etched substrates composed of preferentially oriented rod-shaped fluoroapatite (FAP) crystals interspersed in a silica matrix were sampled out after different reaction times, rinsed with deionized water, dried with canned air and analyzed (Ref 11, <sup>24</sup>).



Atomic force microscopy (AFM, *Nanoscope III, Digital Instruments*) and Scanning Electron Microscopy (SEM, *DS130C, Topcon*) were used for the morphological characterization of the samples. The samples from static experiments were prepared for the AFM analysis by extracting a droplet of the suspension and depositing on a glass slide, keeping it for 1h in a wet cell, washing with a few droplets of water and drying with canned air. Tapping-mode AFM was applied using Si-tips with a radius of about 5 nm (*Supersharpe, Nanosensors*). Selected samples were sputtered with gold and studied on the SEM at 5 kV. Energy-disperse analysis (EDX, *DX-4, Topcon*) was applied to determine the presence of calcium, phosphate and carbon. Protein solutions were analyzed at different time points of MMP-20 digestion using Matrix-assisted laser desorption ionization time-of-flight (MALDI-TOF) mass spectrometry (*Voyager DE STR, Applied Biosystems*). To analyze solution digests, MMP-20 in concentration of 200 nM was added to a solution composed of an assay buffer (10 mM CaCl<sub>2</sub>, 150 mM NaCl, 10 mM ZnCl<sub>2</sub> and 50 mM Tris/HCl at pH 7.5) and 2.0 mg/ml rH174. To analyze digestion of Amg bound to carbonated apatite (obtained using a previously described method<sup>15</sup>), 200 μL of the assay buffer along with 3 μL (200 nM) of MMP-20 was added to a suspension composed of 1 and 2 mg/ml of carbonated apatite and rH174, respectively, in 20 mM Tris/HCl aqueous buffer at pH 7.5. In both cases, the proteolytic reaction was stopped by the addition of 1.0% formic acid and 50% acetonitrile. The samples were then diluted with 0.1% formic acid to a final concentration of 1.4 pmol/μl and mixed with a matrix ( $\alpha$ -cyano-4-hydroxycinnamic acid in 50% acetonitrile and 0.3% tetrafluoric acid, 5 mg/ml) in a 1:1 ratio directly on the stainless steel target. Ionic content analyses (Ca<sup>2+</sup>, PO<sub>4</sub><sup>3-</sup>) of supernatant solutions were done by means of atomic absorption spectrometry (*Perkin Elmer 3110*) and atomic spectrophotometry (*Milton Roy, Genesys 5*).

## Results and Discussion

### a) Self-assembly of rH174 and its proteolytic cleavage products in static conditions

Aqueous suspensions of rH174 (0.1 mg/ml) result in the formation of uniform spherical aggregates with 20 – 30 nm in size on average, as shown in Fig.4a. The stability of these dispersions was evidenced by the lack of agglomeration and retained spherical shapes of the particles even after prolonged incubation at the physiological conditions. On the other hand, rH163 (the recombinant variant of rH174 with its sequence corresponding to the one formed by cleaving off the C-terminal of the nascent molecule) forms nanospheres of a similar size as rH174 at pH around 7.4 (Fig.4b). However, when rH174 and rH163 were mixed together, alignment of these nanospheres into short strings was observed within a relatively short incubation time (24 h). The strings reached a length of up to 300 nm and were often connected with another. High resolution imaging revealed that the nanostrings consisted of segments (Fig. 4c), indicating that a coalescence of the primary spheres is responsible for the formation of these elongated assemblies. The formation of higher order structures of mixtures of the full-length amelogenin protein with one of its cleavage products indicates the importance of protein processing for the development of supramolecular structures that might be crucial in the hypothesized fiber-to-fiber guided growth of apatite crystals in-vivo.

The results of a mass-spectrometric analysis of the enzymatic cleavage of rH174 by MMP-20 are shown in Fig.5. The initial rH174 solution comprises the pure protein, the main peak of which is detected at 19.8 kDa. The cleavage products appear within the first 10 minutes of hydrolysis. While a peak at 18.5 kDa corresponding to the Amg fragment lacking 11 amino acids at its C-terminal (rH163) and a peak at 5 kDa corresponding to the tyrosine-rich Amg fragment (TRAP) increase in intensity over the hydrolysis time, the peaks attributed to the full-length protein (rH174) decrease and become barely visible after one hour of the reaction time. However, there is a higher rate of the proteolytic hydrolysis of Amg molecules observed when they are bound to an apatite surface comparing to the reaction in solution. Whereas it takes



more than 30 min for MMP-20 to completely process Amg in the solution, the same process comes to completion in less than 10 min in the presence of the mineral phase. This observation adds up to the thesis that the self-assembly of Amg matrix into biologically relevant morphologies becomes fostered in the presence of the components of the mineral phase.

Morphologies of the peptide aggregates obtained by mixing rH174 and MMP-20 differ from the ones observed in the absence of MMP-20 (Figs.6–7). Moreover, different incubation pHs result in different morphologies and aggregation tendencies and rates, signifying that the described process is pH-sensitive. The proteolytic reaction at mild acidic conditions results in the morphologies that differ from the typically spherical particles observed at neutral pH conditions. The formation of ring-shaped aggregates, continuous mesh-like assemblies and smooth layers, altogether with a wider dispersion of the protein particle sizes indicates an ostensible influence of MMP-20 on the assembly of Amg nanospheres during their aging under the given conditions. For example, at pH 5.5, a population of spherical peptide particles reaching up to two micrometers in diameter was observed as dispersed within a large number of peptide spheres with 200 – 300 nm in size (Fig.6a). A higher resolution image revealed multi-scale ripening effects as all particles, irrespective of their size turned out to be composed of smaller spherical entities, the smallest one of which had 30 – 50 nm in size (Fig.6b). It was previously reported that Amg fragments that lack the C-terminal have a tendency for the formation of larger aggregates, including micrometer sized particles, owing to less charged colloid peptide entities and, henceforth, a decreased repulsion in their electrostatic interaction<sup>16,17</sup>.

However, whereas Amg assemblies of comparatively larger sizes and a wider distribution thereof were observed predominantly at acidic pHs, the suspensions incubated at conditions close to neutral pH retained an equally narrow particle size distribution throughout the entire 7-day incubation periods. This indicates that stability of the spherical Amg assemblies may be enhanced at the physiological conditions of pH, temperature and ionic strength. Protein strings extending up to a micron in length were detected only at pH ~ 7.6 after a week of incubation (Figs.7b–c). These strings, furthermore, appear as if formed through an alignment and fusion of the individual nanospheres, the sizes of which do not change with aging.

Another indicator of the MMP-20 activity is a decreased amount of the deposited protein as the incubation time is prolonged under most of the analyzed pH conditions. This effect is correlated with the smaller size and a higher solubility of the sum of peptide species formed following the cleavage of the nascent molecule.

It is important to note that the identified self-assembled morphologies do not necessarily imply their presence in the relevant biological environment. On the other hand, a consistent formation of elongated protein assemblies may present an incentive towards revisiting the basic paradigm used for explaining the interaction between Amg and HAP during amelogenesis, suggesting that a co-alignment of the protein assemblies and the HAP particles may be the major mechanism of amelogenesis.

## b) Continuous Crystallization Experiments

In order to provide referential experiments for a more reliable insight into the effect MMP-20 has on the self-assembly of rH174 in the presence of the precipitation of HAP, control experiments that excluded the presence of MMP-20 were carried out. Morphological changes over a 7-day period in a representative experiment are shown in Fig.8. A gradual transformation from uniform and isolated 30 to 40 nm sized particles (taking into account the tip broadening effect, the size of the nanospheres could be estimated as in the range of 20 – 30 nm) to their gradual merging and subsequent formation of individual fibrils to the eventual formation of a loose fibrous mesh was observed.

In the course of a typical continuous crystallization experiment involving the presence of MMP-20, the morphology of Amg assemblies similarly changes from spherical particles interconnected so as to form strings to the one of a fibrous mesh (Fig.9). As the same transition was hardly noticeable in the absence of calcium phosphate titration, it seems as if it becomes fostered in the presence of the continuous supply of calcium and phosphate ions in the solution. However, that these fibrous morphologies are primarily peptide-based can be evidenced from the results of an SEM-EDX analysis, shown in Fig.10.

Although the cleavage of rH174 and its fragments by the action of MMP-20 is expected to take place practically momentarily, the subsequent interlinking of the resulting protein aggregates and the formation of a continuous fibrous network occurs gradually over time. Whereas short strings of amelogenin were observed within 24 hours of the continuous crystallization experiment in the presence of MMP-20, such elongated entities did not appear until after three days of the reaction time in the absence of the protease. However, the formation of Amg fibers and meshes was observed in both types of continuous crystallization experiments: the ones that excluded (Fig.8) and the ones that included MMP-20 (Fig.9).

The results of the analysis of calcium and phosphate ions concentrations in the supernatant solutions from a set of experiments are displayed in Fig.11. Whereas the ionic concentrations are apparently subject to variations, it can be noted that, in general, they maintain the values in close proximity with the initial ones, set forth using the calculations described in the experimental section. Only minor fluctuations in the ionic concentrations were detected in the experiment performed in the absence of the protein matrix. Calcium and phosphate concentrations varied by about 15%. With the addition of 0.4 mg/ml rH174, the calcium and phosphate concentrations, however, become much more variable, and a similar trend was observed upon the addition of MMP-20 to the system. All protein-containing solutions showed a gradual decrease in the free calcium concentration over time. As shown in Fig.11, calcium continues to drop and reaches values as low as 0.8 mM after six days, which is half of its initial concentration. In the presence of MMP-20, the reduction of free calcium ions was even more drastic, reaching as low as 0.4 mM after seven days. The phosphate concentration of the supernatant showed less variations, but an overall trend of decreasing with time was frequently observed, although some samples displayed an opposite trend of increased phosphate content later in the process. This effect is attributed to the dissolution of the glass matrix of the glass-ceramic composite comprising the substrates<sup>18</sup>.

Table 1 summarizes the data obtained from continuous crystallization experiments in the presence and absence of 0.4 mg/ml rH174 and MMP-20. Despite the variations in the ionic concentrations, the degree of saturation did not exhibit significant fluctuations. Most importantly, saturation of the reaction solutions was maintained under metastable conditions in all experiments. Neither was the level of spontaneous crystallization surpassed nor the solutions undersaturated with respect to HAP indicating apatite dissolution.

Overall, it is a general trend for the ionic concentration to decrease as the proportion of the peptide species in the system is raised. The detected consumption of calcium ions during the process may be explained by their complexation with specific Amg side chains (e.g., aspartic acid). Despite its predominantly hydrophobic nature, Amg belongs to the same group of proline-rich proteins as most proteins in human parotid and submandibular saliva known for their ability to bind calcium and thus assist in maintaining the concentration of ionic calcium in saliva constant<sup>19,20</sup>. A previous study reported a sequestration of calcium ions by rH174, resulting in approximately 6 calcium ions bound to a single rH174 molecule<sup>21</sup>. The fact that the sequestration effect is even more pronounced in the experiment with the protein matrix composed of proteolytically processed rH174 may be explained by an increased exposure of amino acid residues following the proteolytic cleavage. The same study came to the conclusion



that some of the splice products of the nascent Amg may even have a higher affinity for calcium ions comparing to the aggregates of rH174. Such is, for example, the case of leucine-rich Amg peptide whose calcium affinity is measured as 6 times higher comparing to that of the full-length Amg. Nevertheless, the observed instability of ionic concentrations in the continuous crystallization experiments provides an additional support for the assumed mineral-assisted self-assembly of biologically relevant Amg morphologies.

The titration rates were very slow and in the order of 2 – 30  $\mu\text{l}$  per hour for all the experiments. These rates are comparable to the ones achieved by cells in the course of an active regulation of ionic concentration (including pH) in the extracellular matrix. In general, the titration rates became lower when rH174 was present in the system and even further reduced when MMP-20 was additionally introduced. A reduction in the titration rates implied a reduced crystal growth and nucleation. This observation is in agreement with previous studies that have shown that Amg due to its predominantly hydrophobic nature does not provide a convenient nucleation-promoting surface<sup>22</sup>. Moreover, Amg may be involved in blocking the nucleation sites on the FAP crystals of the substrate by adhering to their surface. This observation is in contrast to other studies showing that Amg promotes nucleation of apatite at relatively low protein concentrations<sup>23,24,25</sup>. Interestingly, the proteolytic processing of rH174 seems to additionally inhibit crystallization events, as indicated by the lowest titration rates detected in the experiments that involved the presence of MMP-20. The proteolytic cleavage of rH174 creates a number of highly hydrophobic molecules which would even more efficiently block the nucleation sites by adsorption onto the FAP substrates.

After all, there are reasons to expect that not only Amg assemblies conduct the growth of the mineral phase, but that the constituents of the mineral phase are similarly essential for the proper assembly of the protein phase<sup>26</sup>. The results presented hereby provide a support for the previously hypothesized idea that simultaneous co-assembly of the peptide and mineral phases takes place in the course of amelogenesis<sup>27,28,29,30</sup>. Self-assembly of other proteins and organic molecules has been previously demonstrated as dependent on the supply of calcium ions<sup>31</sup>.

As far as the preferential surface nucleation and the consequent epitaxial crystallization are concerned, no significant differences were observed by comparing the crystal growth over the apatite crystals of the substrate after or during any of the continuous crystallization experiments (in the absence of the protein matrix, in the presence of rH174 alone, and in the presence of both peptide components - rH174 and MMP-20), as shown in Fig.12. However, these experiments were performed at protein concentrations significantly lower comparing to the ones in the enamel matrix. Amg concentration in the latter is 200 – 300 mg/ml, which is by almost three orders of magnitude higher than in our experiments<sup>31</sup>. As pointed out in a previous study<sup>32</sup>, a more significant rate of the crystal growth was noticed only in the presence of rH174 at concentrations that exceeded its solubility limit of approximately 0.8 mg/ml. The formation of a gel-like matrix, resembling the dense and highly viscous conditions of the enamel matrix, may be required to induce and guide nucleation and growth of enamel-like apatite crystals. The future studies aim at exploring the synergy between the protein assembly, the proteolytic interaction and the crystal growth at notably higher protein concentrations.

## Conclusions

The formation of more complex self-assembled morphologies comparing to the standard nanospheres is facilitated under conditions wherein either: a) rH174 and the first MMP-20 cleavage product (rH163) are present in the suspension; b) proteolytic cleavage by the action of MMP-20 is coupled with the self-assembly of the protein matrix composed of rH174; or c) mineral growth takes place simultaneously with the self-assembly of the protein matrix. The

process of amelogenesis is crucially dependent on the presence of MMP-20, since the enzymatic hydrolysis will generate protein fragments that accelerate the cooperative self-assembly of matrix proteins into fibrillar structures that may facilitate anisotropic apatite growth. A central outcome of this study is the notion that a synergy between protein assembly, proteolysis and crystallization is required for the mimicry of amelogenesis *in-vitro* in a cell-free environment. Bioimitational growth of enamel will likewise depend on the abilities to control the coordination of these three elements of the process. The experimental setup based on a feedback-controlled delivery of precipitating ions to the self-assembling protein matrix could present a convenient starting point for both understanding the mechanism of amelogenesis at the nano-scale and gaining control over the organic/inorganic interactions of interest. As such, it may bring forth crucial steps on the way towards the ideal of the biomimetic synthesis or regeneration of dental enamel *in vitro*.

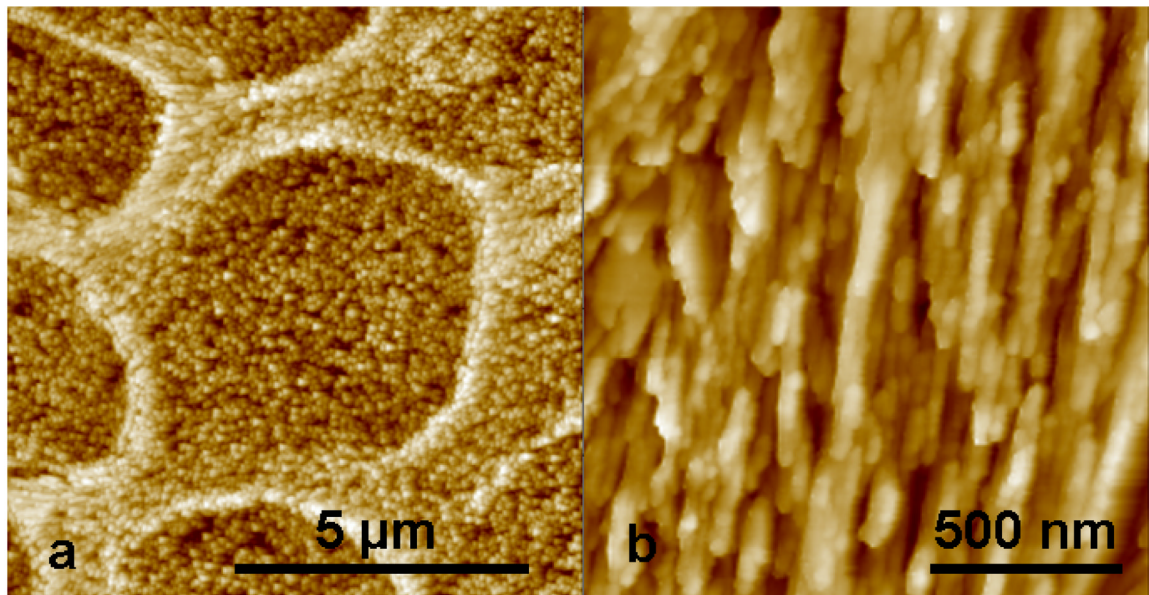
## Acknowledgements

The presented study was supported by NIH/NIDCR grants R01-DE17529 and R01-DE015821. The authors acknowledge the assistance of Xiaodong He for providing the AFM images of the assembly of pure rH174 and rH163 suspensions and H. Ewa Witkowska, Sarah Robinson, Venu Varanasi, Markus Hardt and Steve Hall for the MALDI-TOF analyses. The UCSF Biomolecular Resource Center Mass Spectrometry facility was supported by a grant from the Sandler New Technology Fund.

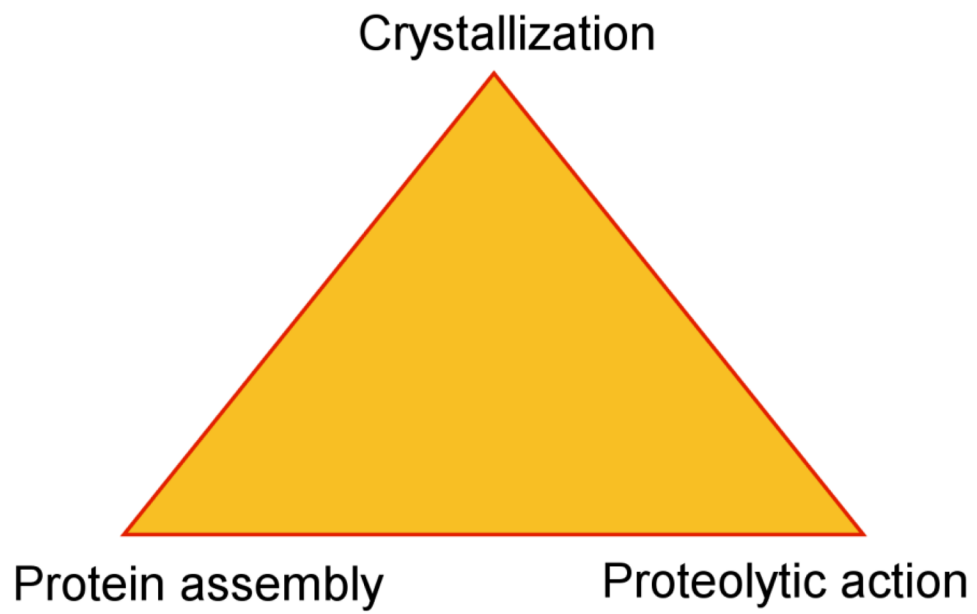
## References

- Garant, PR. Oral Cells and Tissues. Quintessence; Carol Stream, IL: 2003.
- Bartlett JD, Ryu OH, Xue J, Simmer JP, Margolis HC. Enamelysin mRNA Displays a Developmentally Defined Pattern of Expression and Encodes a Protein which Degrades Amelogenin. *Connective Tissue Research* 1998;39:405–413.
- Moradian-Oldak J, Du C, Falini G. On the Formation of Amelogenin Microribbons. *European Journal of Oral Sciences* 2006;114(Suppl 1):289–296. [PubMed: 16674701]
- Du C, Falini G, Fermani S, Abbott C, Moradian-Oldak J. Supramolecular Assembly of Amelogenin Nanospheres into Birefringent Microribbons. *Science* 2005;307:1450–1454. [PubMed: 15746422]
- Wiedemann-Bidlack FB, Beniash E, Yamakoshi Y, Simmer JP, Margolis HC. pH Triggered Self-Assembly of Native and Recombinant Amelogenins under Physiological pH and Temperature *in vitro*. *Journal of Structural Biology* 2007;160:57–69. [PubMed: 17719243]
- Bartlett JD, Simmer JP. Proteinases in Developing Enamel. *Critical Reviews in Oral Biology and Medicine* 1999;10(4):425–441. [PubMed: 10634581]
- Bartlett JD, Skobe Z, Lee DH, Wright JT, Li Y, Kulkarni AB, Gibson CW. A Developmental Comparison of Matrix Metalloproteinase-20 and Amelogenin Null Mouse Enamel. *European Journal of Oral Sciences* 2006;114(Suppl 1):18–23. [PubMed: 16674657]
- Caterina JJ, Skobe Z, Shi J, Dang Y, Simmer JP, Birkedal-Hansen H, Bartlett JD. Enamelysin (MMP-20) Deficient Mice Display an Amelogenesis Imperfecta Phenotype. *Journal of Biological Chemistry* 2002;277(51):49598–49604. [PubMed: 12393861]
- Li W, Gao C, Yan Y, DenBesten PK. X-linked amelogenesis imperfecta may result from decreased formation of tyrosine rich amelogenin peptide (TRAP). *Archives in Oral Biology* 2003;48:177–183.
- Tomson MB, Nancollas GH. Mineralization Kinetics; A Constant Composition Approach. *Science* 1978;200:1059–1060. [PubMed: 17740700]
- Habelitz S, DenBesten PK, Marshall SJ, Marshall GW, Li W. Amelogenin Control over Apatite Crystal growth is Affected by the pH and Degree of Ionic Saturation. *Orthodontics and Craniofacial Research* 2005;8:232–238. [PubMed: 16238603]
- McDowell H, Gregory TM, Brown WE. Solubility of  $\text{Ca}_5(\text{PO}_4)_3\text{OH}$  in the System  $\text{Ca}(\text{OH})_2\text{-H}_3\text{PO}_4\text{-H}_2\text{O}$  at 5, 15, 25 and 37.5 °C. *J Res Natl Bur Stand* 1977;81A:273–281.
- Larsen, MJ. Ion Products and Solubility of Calcium Phosphates. Royal Dental College; Denmark: 2001.

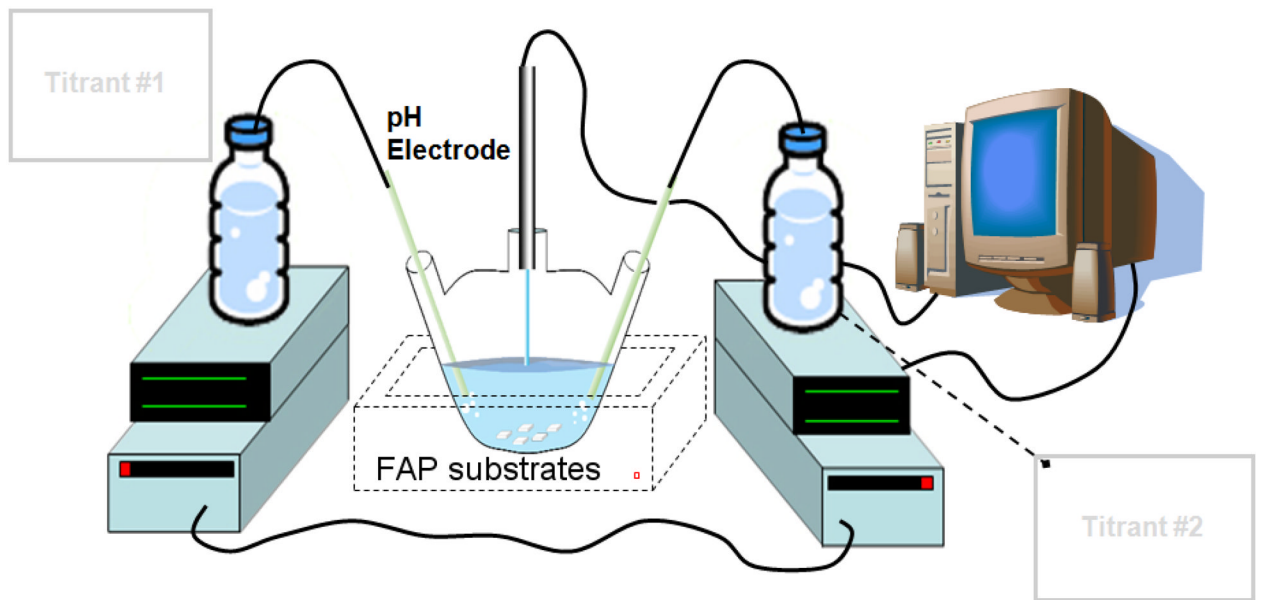
14. Koutsoukas P, Amjad Z, Tomson MB, Nancollas GH. Crystallization of Calcium Phosphates. A Constant Composition Study. *Journal of the American Chemical Society* 1980;102:1553–1557.
15. Featherstone JD, Mayer I, Driessens FC, Verbeeck RM, Heijligers HJ. Synthetic Apatites Containing Na, Mg, and CO<sub>3</sub> and their Comparison with Tooth Enamel Mineral. *Calcified Tissue International* 1983;35:169–171. [PubMed: 6850399]
16. Moradian-Oldak J. Amelogenins: Assembly, Processing and Control of Crystal Morphology. *Matrix Biology* 2001;20:293–305. [PubMed: 11566263]
17. Beniash E, Simmer JP, Margolis HC. The Effect of Recombinant Mouse Amelogenins on the Formation and Organization of Hydroxyapatite Crystals in vitro. *Journal of Structural Biology* 2005;149(2):182–190. [PubMed: 15681234]
18. Hoche T, Moisescu C, Avramov I, Russel C, Heerdegen WD, Jager C. Microstructure of SiO<sub>2</sub>-Al<sub>2</sub>O<sub>3</sub>-CaO-P<sub>2</sub>O<sub>5</sub>-Na<sub>2</sub>O-K<sub>2</sub>O-F Glass Ceramics. 2. Time Dependence of Apatite Crystal Growth. *Chemistry of Materials* 2001;13:1320–1325.
19. Bochicchio B, Tamburro AM. Polyproline II Structure in proteins: Identification by Chiroptical Spectroscopies, Stability, and Functions. *Chirality* 2002;14:782–792. [PubMed: 12395395]
20. Rath A, Davidson AR, Deber CM. The Structure of ‘Unstructured’ Regions in peptides and Proteins: Role of the Polyproline II Helix in Protein Folding and Recognition. *Biopolymers* 2005;80:179–185. [PubMed: 15700296]
21. Le TQ, Gochin M, Featherstone JDB, Li W, DenBesten PK. Comparative Calcium Binding of Leucine-Rich Amelogenin Peptide and Full-Length Amelogenin. *European Journal of Oral Sciences* 2006;114(Suppl 1):320–326. [PubMed: 16674706]
22. Hunter GK, Curtis HA, Grynopas MD, Simmer JP, Fincham AG. Effects of Recombinant Amelogenin on Hydroxyapatite Formation in vitro. *Calcified Tissue International* 1999;65:226–231. [PubMed: 10441656]
23. Wang L, Guan X, Du C, Moradian-Oldak J, Nancollas GH. Amelogenin Promotes the Formation of Elongated Apatite Microstructures in a Controlled Crystallization System. *Journal of Physical Chemistry C* 2007;111(17):6398–6404.
24. Wang L, Guan X, Yin H, Moradian-Oldak J, Nancollas GH. Mimicking the Self-Organized Microstructure of Tooth Enamel. *Journal of Physical Chemistry C* 2008;112(15):5892–5899.
25. Tarasevich BJ, Howard CJ, Larson JL, Snead ML, Simmer JP, Paine M, Shaw WJ. The Nucleation and Growth of Calcium Phosphate by Amelogenin. *Journal of Crystal Growth* 304(2):407–415. [PubMed: 19079557]
26. Uskoković V. Isn't Self-Assembly a Misnomer? Multi-Disciplinary Arguments in Favor of Co-Assembly. *Advances in Colloid and Interface Science* 2008;141(1–2):37–47. [PubMed: 18406396]
27. Cölfen H, Mann S. Higher-Order Organization by Mesoscale Self-Assembly and Transformation of Hybrid Nanostructures. *Angewandte Chemie International Edition: English* 2003;42:2350–2365.
28. Fearnhead RW. The Electron Microscopy of Amelogenesis in the Rat. *Journal of Dental Research* 1960;39:1104.
29. Eastoe JE. The Amino Acid Composition of Proteins from the Oral Tissues. *Archives in Oral Biology* 1963;52:633–652.
30. Margolis HC, Beniash E, Fowler CE. Role of Macromolecular Assembly of Enamel Matrix Proteins in Enamel Formation. *Journal of Dental Research* 2006;85(9):775–793. [PubMed: 16931858]
31. Tourbez M, Firanescu C, Yang A, Unipan L, Duchambon P, Blouquit Y, Craesu CT. Calcium-Dependent Self-Assembly of Human Centrin 2. *Journal of Biological Chemistry* 2004;279(46):47672–47680. [PubMed: 15356003]
32. Habelitz S, Kullar A, Marshall SJ, DenBesten PK, Balooch M, Marshall GW, Li W. Amelogenin-guided Crystal Growth on Fluoroapatite Glass-Ceramics. *Journal of Dental Research* 2004;83(9):698–702. [PubMed: 15329375]



**Fig.1.** AFM images of the microstructure of human enamel: Key-hole-shaped enamel rods of about 5  $\mu\text{m}$  diameter run from the dentin-enamel junction to the surface of the tooth (a) and are comprised of aligned apatite crystals 40 to 60 nm wide and several hundreds of micrometers long (b).

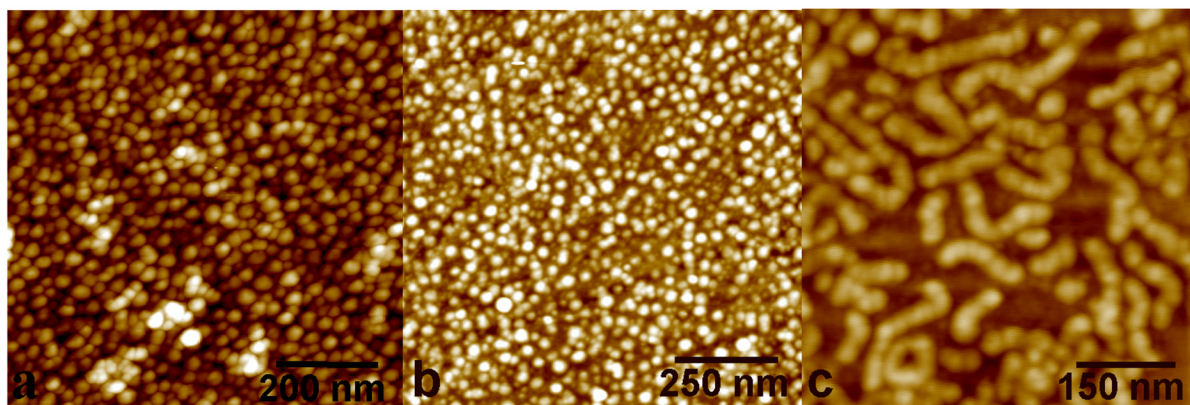


**Fig.2.** Schematic illustration of the synergy between the three aspects of the process of amelogenesis: Amg self-assembly, proteolysis and crystallization.

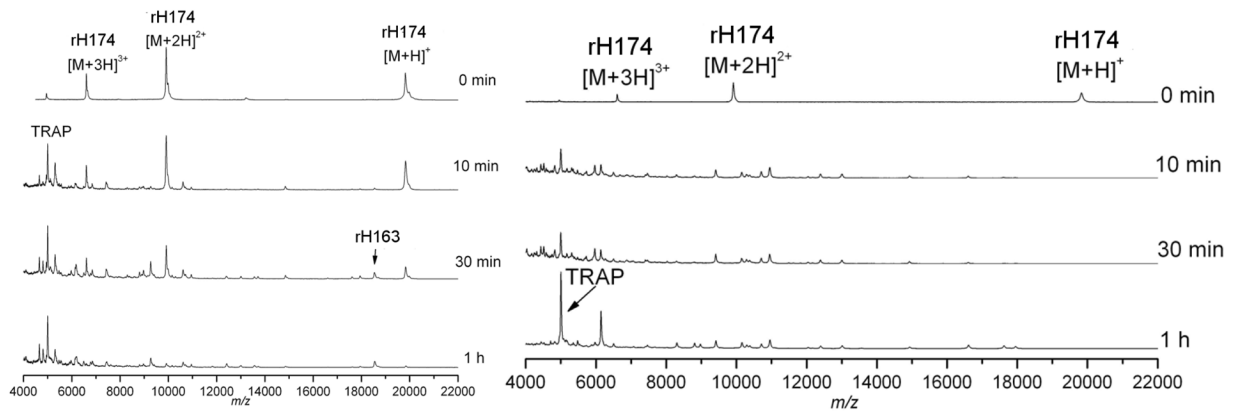


**Fig.3.** Scheme of the “continuous crystallization” experimental setup for a controlled precipitation of the apatite phase in the presence of protein matrix and MMP-20.

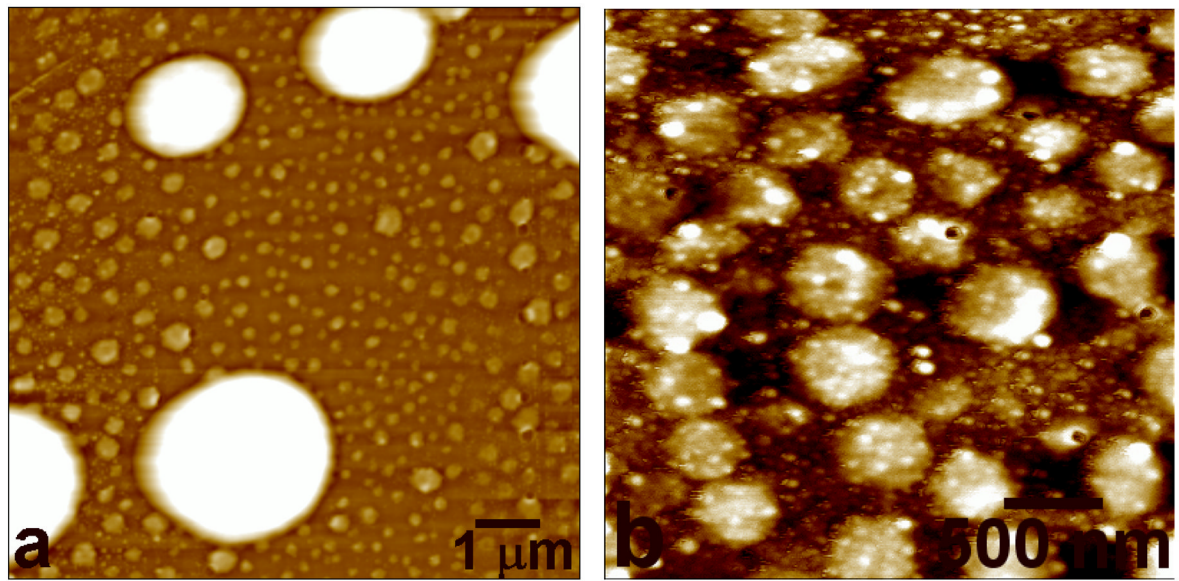




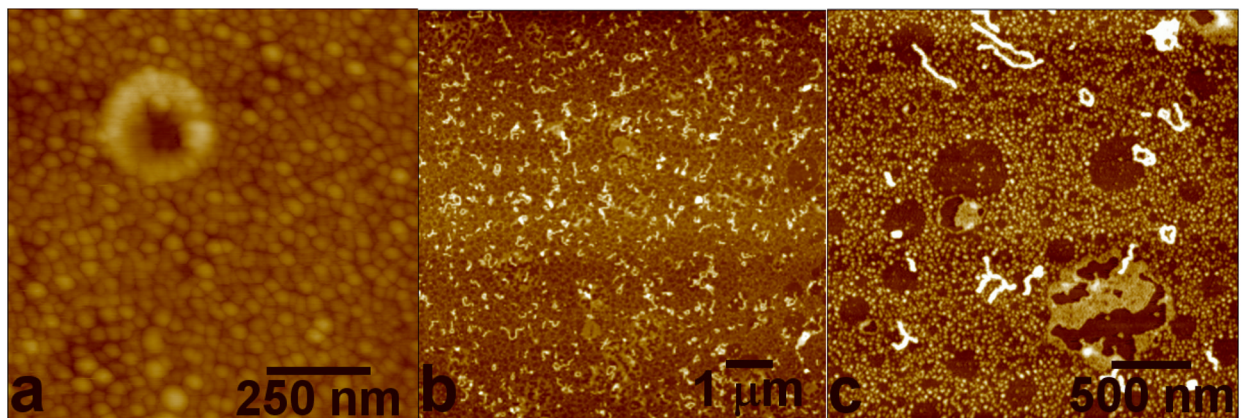
**Fig.4.** AFM images of uniform spheres of rH174 dispersed in water (0.1 mg/ml) at pH 7.4, after the incubation time of 24 h (a); similarly uniform spheres of rH163 obtained at pH 7.4 and after an equal incubation time (b); and nanostrings formed in aqueous mixtures of rH174 and rH163 at pH 7.4 in 1:1 weight ratio (c).



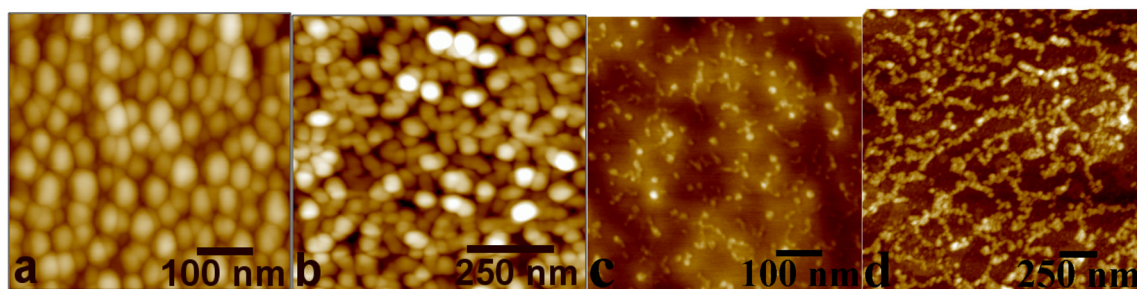
**Fig.5.** MALDI-TOF mass spectrograms illustrating the time-course of the proteolytic reaction between MMP-20 and rH174 nanospheres dispersed in water at pH 7.5 (left) and when rH174 was bound to a carbonated HAP surface (right).



**Fig.6.** Amg assemblies formed 27 h after the initiation of the hydrolysis of rH174 by the action of MMP-20 at pH = 5.5. Note that the aggregation of smaller spherical subunits leads to the formation of larger spheres with the consequent broadening of the aggregate size distribution.

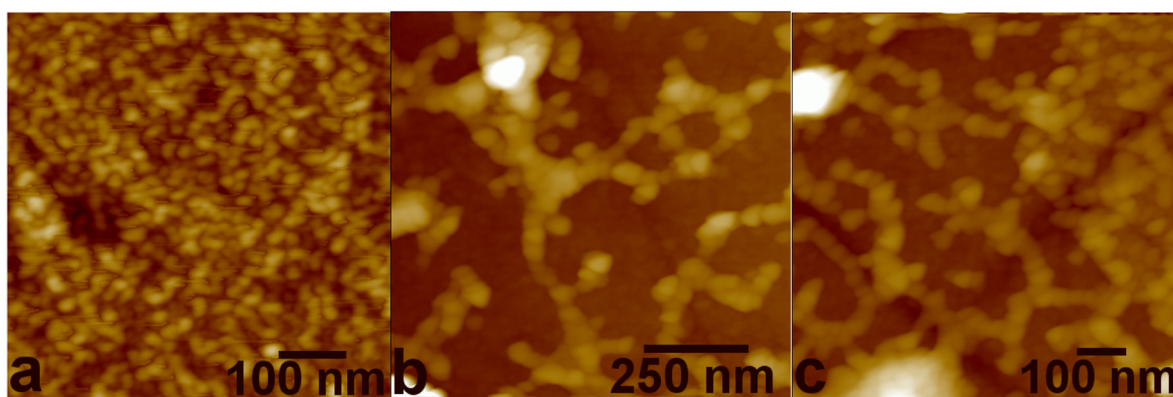


**Fig.7.** Amg assemblies formed in the static proteolytic experiment at pH 7.6, sampled out after 1h (a) and 7 days (b, c) of the incubation time. Note the narrow size distribution and discrete nature of the particles formed after the short aging time (a), and the co-existence of similarly discrete particles and protein strings obtained after the prolonged aging (b, c).



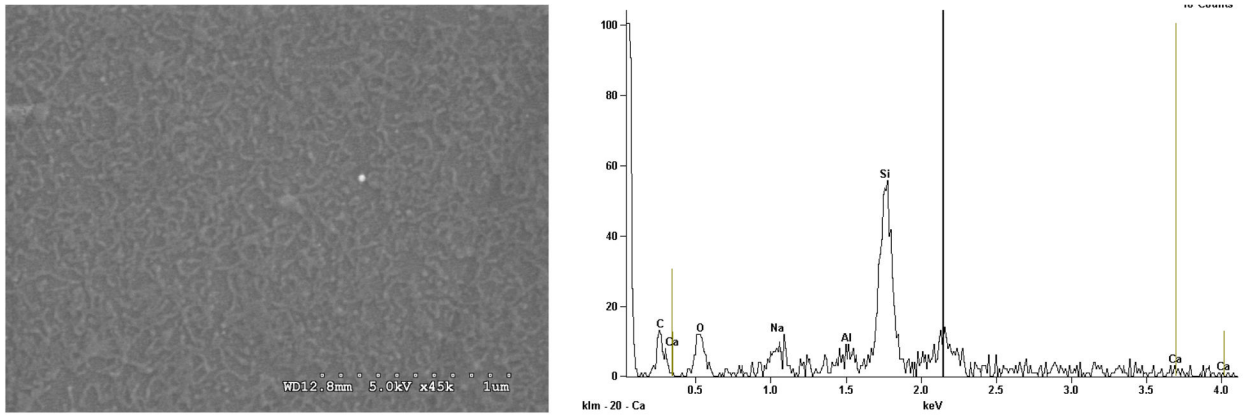
**Fig.8.** AFM micrographs of Amg assemblies from a continuous crystallization experiment without the presence of MMP-20, obtained after 15 min (a), 18 h (b), 3 days (c), and 7 days (d) of the reaction time.



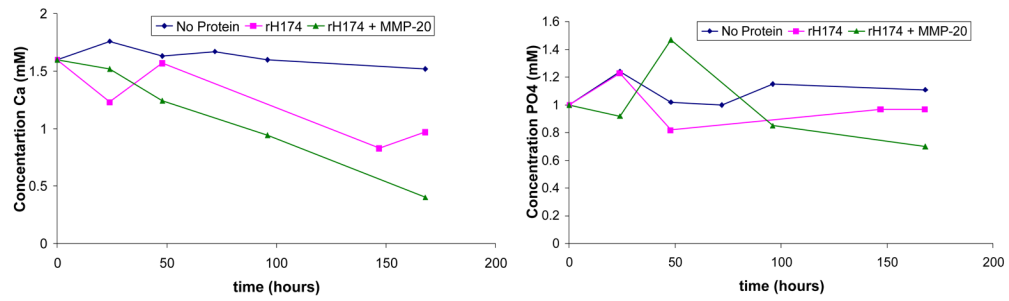


**Fig.9.** AFM micrographs of Amg assemblies from a continuous crystallization experiment involving the presence of MMP-20, obtained after 1 (a), 6 (b), and 7 days (c) of the reaction time.

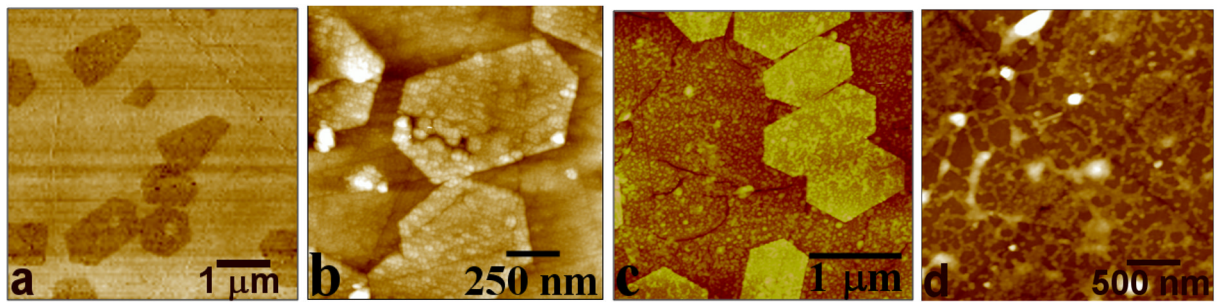




**Fig.10.** SEM micrograph of self-assembled rH174 (left) with the EDX elemental analysis of the surface (right), showing the presence of silica, sodium, aluminum and carbon, but the lack of calcium and phosphate.



**Fig.11.** Concentrations of calcium and phosphate ions in the supernatant solutions after different reaction times of a continuous crystallization experiment with and without the presence of rH174 and MMP-20.

**Fig.12.**

A polished nucleation substrate composed of preferentially oriented FAP crystals interspersed in a silica matrix, with (001) apatite surfaces lying a few nanometers below the level of the matrix in the initial conditions (a). The FAP substrate after 120 h of remaining in the solution without the protein matrix in the course of a continuous crystallization titration (b), after 145 h of continuous crystallization with the protein matrix composed of 0.4 mg/ml rH174 (c), and after 160 h of continuous crystallization with the protein matrix composed of rH174 and MMP-20. In all cases the mineral grew up to about 20 nm above the level of the surrounding silica glass (d). Notice the protein spheres and fibers interspersed around the crystals grown in MMP-20-free (c) and MMP-20-comprising (d) Amg solutions, respectively, comparing to the flat silica surfaces of the samples (a) and (b).

**Table 1**  
Titration and ionic parameters throughout the 7-day continuous crystallization experiments in the presence and absence of 0.4 mg/ml rHI174 and MMP-20.

Time	Day 1		Day 4		Day 7	
	rHI174	rHI174 +MMP20	rHI174	rHI174 +MMP20	rHI174	rHI174 +MMP20
Proteins	None	6-9	None	2-5	None	<15
Titration Rates (ul/h)	24-26	5-27	19-25	3-15	19-21	<4
DS <sub>HAP</sub>	11.3	10.3	11.1	10.5	10.8	9.2
		10.6		9.5		7.5